Simulation of single bubble dynamic process in pool boiling process under microgravity based on phase field method

Chang-Sheng Zhu(朱昶胜)[1,2,†], Bo-Rui Zhao(赵博睿)[1], Yao Lei(雷瑶)[1], and Xiu-Ting Guo(郭秀婷)[1]

[1] *College of Computer and Communication, Lanzhou University of Technology, Lanzhou* 730050, *China*

[2] *State Key Laboratory of Gansu Advanced Processing and Recycling of Non-Ferrous Metal, Lanzhou University of Technology, Lanzhou* 730050, *China*

(Received 2 August 2022; revised manuscript received 30 October 2022; accepted manuscript online 11 November 2022)

We use the phase field method to track the gas–liquid interface based on the gas–liquid two-phase flow in the pool boiling process, and study the bubble nucleation, growth, deformation, departure and other dynamic behaviors on the heating surface under microgravity. By simulating the correlation between liquid undercooling and bubble dynamics, we find that the bubble growth time increases with the increase of liquid undercooling, but the effect of liquid undercooling on bubble height is not significant. Meanwhile, the gas–liquid–solid three-phase contact angle and the gravity level will also have an effect on the bubble growth time and bubble height. With the increase of the contact angle, the bubble growth time and bubble height when the bubble departs also increase. While the effect of gravity level is on the contrary, the smaller the gravity level is, the larger the bubble height and bubble growth time when the bubble separates.

Keywords: pool boiling, single-bubble, phase-field method, low-gravity

PACS: 47.11.–j, 47.55.dd **DOI:** 10.1088/1674-1056/aca209

1. Introduction

The boiling process has great heat transfer capacity due to the release of phase change latent heat. With the development of aerospace technology, the application of high-power and highly integrated equipment has been paid more and more attention. The significance of relevant research on boiling heat transfer process for such equipment in cooling and other aspects makes the gas–liquid two-phase heat exchange system technology gradually attract attention.[1] Because of its great application value in aerospace experiments, the study of boiling heat transfer under microgravity has become the focus of research. Specifically, single bubble boiling heat transfer is of great significance as the basis of related research on boiling heat transfer.[2,3]

Boiling heat transfer under microgravity has become one of the key points of microgravity physics experiments. Qiu *et al.*[4] conducted an experimental study on the growth and separation of a single bubble on the heating surface. The experimental result shows the bubble growth cycle is very sensitive to liquid supercooling. Straub *et al.*[5] showed through their research results that boiling can be used as the heat transfer mechanism in the microgravity condition, and the heat transfer coefficient obtained in microgravity is almost the same as that in normal gravity. In addition, the decrease of gravity will reduce the critical heat flux. Lee *et al.*[6] used a high-speed CCD camera to capture the geometry of the bubble growth process, so as to observe and analyze the bubble growth process, and obtained the relevant data of a single bubble in the pool with constant temperature at the boundary during the growth process. Henry *et al.*[7] used heaters with different aspect ratios to carry out pool boiling heat transfer measurements at low microgravity levels, and analyzed the reasons for the expansion and contraction of bubble surfaces under high and low undercooling. Zhao *et al.*[8] conducted a pool boiling experiment in microgravity on the Chinese recoverable satellite SJ-8 by using transient heating, and studied the transition from nuclear to film boiling mode at different degrees of subcooling. Dhir *et al.*[9] conducted experiments on the initiation and growth of a single bubble and the lateral merger and department of multiple bubbles under microgravity. Nejati *et al.*[10] used a laser beam to generate steam bubbles in the supercooled liquid pool in the international space station and explored the effect of laser heat on bubble growth. The result shows that the preheating time has a significant effect on bubble growth. However, the requirements of the above experiments for low microgravity lead to high test cost, long experiment time-consuming and prime requirements for experiment operation. It is difficult to carry out a large number of experimental studies in the international space station, and it is complex to conduct stable low microgravity physical simulation experiments in the ground constant gravity environment.

With the development of computer simulation technology, the numerical simulation method breaks the limitations of the above experimental methods. Li *et al.*[11] adopted the finite difference method and the level set method to simulate the single bubble dynamics during nucleate flow lifting, and the results show that the bulk flow velocity, heat surface orientation, etc., impact bubble dynamics. Pu *et al.*[12] proposed a robust numerical method to simulate the coalescence process

[†]Corresponding author. E-mail: zhucs_2008@163.com

© 2023 Chinese Physical Society and IOP Publishing Ltd

of two bubbles under microgravity and normal gravity conditions, then studied the velocity fields inside and around the bubbles under different gravity conditions. Shu *et al.*[13] used the multi relaxation time-lattice Boltzmann method (MRT-LBM) to study the growth process of bubbles, and analyzed the interaction between different bubbles based on the established model. Urbano and Colin *et al.*[14] used fully resolved numerical simulation to analyze the micro-liquid layer at the bottom of the growing bubble. The results show that if the bubble grows faster than the limit velocity for the contact line, the micro-layer will be formed. Li *et al.*[15] described sharp interface with ghost fluid method, and then simulated the complete single bubble pool boiling process. The research results show that the wall thickness will strongly affect the bubble growth process. Zhang *et al.*[16] further analyzed the influence of the thickness and material parameters of the solid wall on the bubble growth process. Murallidharan *et al.*[17] used direct numerical simulation coupled with an interface tracking method to simulate bubble growth, and compared the bubble growth rate curves obtained from the modeling with the existing experimental data. Liu *et al.*[18] adopted level set methods to use a test function in COMSOL multi physical field software to simulate the single bubble boiling process, and compared the results with the empirical equation of Fritz. Cheng *et al.*[19] simulated the two-dimensional bubble growth under the condition of supercooled nucleate boiling by using the fluid volume method (VOF), and based on this, studied the bubble shape and temperature field. Voglar *et al.*[20] established a simplified physical model that can associate the bubble growth time with other input parameters. The results show that the thickness of the thermal boundary layer has a significant impact on the bubble growth time. Takada *et al.*[21] combined Navier Stokes (NS) equation with phase field model (PFM), proposed NS-PFM calculation method, and applied it to capture the liquid–gas interface motion, providing a better method for interface tracking of two-phase flow. Phase field method is widely used because of its advantages of easy boundary processing, simple programming and good parallelism. Zhu *et al.*[22] simulated the movement of rising bubbles in liquid based on the Cahn–Hilliard phase field model in combination with the phase field method. Wang *et al.*[23] proposed a stabilized phase field method for numerical simulation of boiling heat transfer, and applied this method to the three-dimensional boiling heat transfer. Yi *et al.*[24] conducted numerical simulations of bubble growth under different gravity conditions, and studied the bubble growth behavior under different supercooling. Mianmahale *et al.*[25] used the phase field method to track the interphase between liquid and gas, and studied single bubble electro hydrodynamic effects on the two-phase laminar flow of water under electric field stress. However, although there has a lot of research on boiling heat transfer, there still lacks of research on boiling heat transfer mechanism and bubble dynamic behavior under microgravity, and there has relatively few simulations using phase field method.

In view of above problems, this paper combines the phase field method and uses the phase field function to describe the evolution process of the gas–liquid two-phase free interface. We establish a multi physical field coupling mathematical model including flow field, temperature field and two-phase dynamic interface capture to simulate the dynamic behavior of bubbles in the heated surface and liquid phase from growth to separation from the heated surface in low microgravity environment. Based on the established model, we explore the effects of different undercooling on bubble growth time and bubble height. Meanwhile, we also learn the growth morphology of bubbles and the time when bubbles leave the heated surface when the gravity level is $0.08\boldsymbol{g}$, $0.06\boldsymbol{g}$, $0.04\boldsymbol{g}$, $0.02\boldsymbol{g}$, $0.01\boldsymbol{g}$, $0.008\boldsymbol{g}$, $0.006\boldsymbol{g}$, and $0.004\boldsymbol{g}$, respectively, and expound the rules of bubble growth time and bubble height under different contact angles.

2. Numerical method

In order to simplify the dynamic evolution process of a single bubble on the heating surface and reduce the amount of calculation, we establish a two-dimensional axisymmetric model.

(i) Both gas and liquid phases are incompressible laminar flows.

(ii) The physical properties of the liquid phase are constant, independent of temperature, and the gas conforms to the ideal gas law.

(iii) In this model, the heat transfer equation and the flow control equation are isotropic.

(iv) The model only considers the energy transfer involved in the convection conduction of the flow field, and does not consider the interface radiation heat transfer from the heating interface to the liquid interface.

2.1. Model establishment

In this study, we establish a mathematical model for the single bubble growth process in the boiling process, and we use the phase field method to describe the changes of the two-phase interface in the bubble growth process. In the model, the distribution of gas flow field is described by weakly compressible laminar Navier Stokes equation

$$\begin{aligned}&\rho_{\mathrm{g}}\left(\boldsymbol{v}_{\mathrm{g}}\cdot\nabla\right)\boldsymbol{v}_{\mathrm{g}}+\rho_{\mathrm{g}}\frac{\partial \boldsymbol{v}_{\mathrm{g}}}{\partial t}\\&=\nabla\cdot\left\{\xi_{\mathrm{g}}\left[\nabla\boldsymbol{v}_{\mathrm{g}}+\left(\nabla\boldsymbol{v}_{\mathrm{g}}\right)^{\mathrm{T}}\right]-P_{\mathrm{g}}\boldsymbol{I}-\frac{2\mu(\nabla\cdot\boldsymbol{v})\boldsymbol{I}}{3}\right\}+\boldsymbol{F},\end{aligned}\tag{1}$$

$$\frac{\partial \rho_{\mathrm{g}}}{\partial t}+\nabla\cdot\left(\rho_{\mathrm{g}}\boldsymbol{v}_{\mathrm{g}}\right)=0,\tag{2}$$

where $\boldsymbol{I}$ represents unit vector, t represents time, P represents pressure, μ represents dynamic viscosity, T represents temperature, subscript g represents gas phase, ρ_{g} represents the gas density, $\boldsymbol{v}_{\mathrm{g}}$ represents the gas velocity, ξ_{g} represents the viscosity of the gas phase.

Meanwhile, the distribution of liquid flow field is described by incompressible laminar Navier Stokes equation

$$\begin{aligned}&\rho_{\mathrm{l}}\left(\boldsymbol{v}_{\mathrm{l}}\cdot\nabla\right)\boldsymbol{v}_{\mathrm{l}}+\rho_{\mathrm{l}}\frac{\partial \boldsymbol{v}_{\mathrm{l}}}{\partial t}\\ &=\nabla\cdot\left\{\xi_{\mathrm{l}}\left[\nabla\boldsymbol{v}_{\mathrm{l}}+\left(\nabla\boldsymbol{v}_{\mathrm{l}}\right)^{\mathrm{T}}\right]-P_{\mathrm{l}}\boldsymbol{I}\right\}+\boldsymbol{F}, \qquad (3)\\ &\nabla\cdot\boldsymbol{v}=0, \qquad (4)\end{aligned}$$

where the subscript l represents the liquid phase, ρ_{l} represents the liquid density, $\boldsymbol{v}_{\mathrm{l}}$ represents the liquid velocity, ξ_{l} represents the viscosity of the liquid phase. The volume force of Navier Stokes equation is determined by the gravity term $\boldsymbol{F}_{\mathrm{G}}$ and surface tension $\boldsymbol{F}_{\mathrm{st}}$ of the gas–liquid interface composition[26]

$$\boldsymbol{F}_{\mathrm{st}}=\lambda\left[\frac{\phi\left(\phi^2-1\right)}{h^2}-\nabla^2\phi\right]\nabla\phi, \qquad (5)$$

$$\boldsymbol{F}_{\mathrm{G}}=\rho\boldsymbol{g}_z, \qquad (6)$$

where $\boldsymbol{g}_z$ represents the gravity in the simulation. λ represents the mixed energy density, $h=1.2\times10^{-4}$ m represents the thermocapillary length of the gas–liquid interface thickness, and ϕ represents the phase field variable. And the following relationship exists between the mixing free energy density λ and the surface tension coefficient ϑ:

$$\vartheta=\frac{2\sqrt{2}\lambda}{3h}. \qquad (7)$$

The physical parameters in formula can be defined by the volume ratio of gas and liquid phases, the density ρ can be expressed by the following formula:

$$\rho=\rho_{\mathrm{g}}+\left(\rho_{\mathrm{l}}-\rho_{\mathrm{g}}\right)V_{\mathrm{f}}, \qquad (8)$$

where ρ_{g} and ρ_{l} are the densities of the gas and liquid, respectively. And thermal conductivity k, specific heat C_{p}, and kinetic viscosity μ can all be calculated in a similar way to ρ. Among them, the volume ratio is calculated as follows:

$$V_{\mathrm{f}}=\min(\max([(1+\phi)/2],0),1). \qquad (9)$$

In the simulation process, the natural boundary conditions that should be satisfied on the gas–liquid interface of gas phase and liquid phase are

$$\begin{aligned}\boldsymbol{n}\cdot\left[\xi_{\mathrm{l}}\left[\nabla\boldsymbol{v}_{\mathrm{l}}+\left(\nabla\boldsymbol{v}_{\mathrm{l}}\right)^{\mathrm{T}}\right]-P_{\mathrm{l}}\boldsymbol{I}\right]\boldsymbol{v}&=m\left(\boldsymbol{v}_{\mathrm{l}}-\boldsymbol{v}_{\mathrm{g}}\right)+\vartheta\kappa\boldsymbol{n}\\ &+\boldsymbol{n}\left\{\xi_{\mathrm{g}}\left[\nabla\boldsymbol{v}_{\mathrm{g}}+\left(\nabla\boldsymbol{v}_{\mathrm{g}}\right)^{\mathrm{T}}\right]-\boldsymbol{P}_{\mathrm{g}}\boldsymbol{I}\right\}, \qquad (10)\end{aligned}$$

where $\boldsymbol{n}$ represents the unit normal vector from the liquid phase to the gas phase, κ represents the curvature of the interface. m represents the vaporization rate, and $m=0$ represents there is no phase transition on the interface. Meanwhile, Dirac Delta function is introduced to track the surface tension on the two-phase interface δ, to make sure the surface tension only act on the gas–liquid free interface

$$\delta=6V_{\mathrm{f}}\left(1-V_{\mathrm{f}}\right)\frac{|\nabla\phi|}{2}, \qquad (11)$$

where V_{f} represents the volume ratio, which can be used to solve the physical parameters of the gas–liquid two phases in the domain.

Since the gas–liquid interface changes with time during the evaporation of the liquid phase, the movement speed of the interface, the movement speed of the liquid phase at the interface and the movement speed of the gas phase at the interface should satisfy

$$\boldsymbol{v}_{\mathrm{int}}=\boldsymbol{v}_{\mathrm{l}}-\frac{m}{\rho_{\mathrm{l}}}\boldsymbol{n}, \qquad (12)$$

where $\boldsymbol{v}_{\mathrm{int}}$ represents the interface movement speed, and m represents the vaporization rate. For the gas–liquid phase transition in the boiling process, a continuity equation with phase transition is introduced by the phase field method to describe as

$$\nabla\cdot\boldsymbol{v}=m\delta\left(\frac{1}{\rho_{\mathrm{g}}}-\frac{1}{\rho_{\mathrm{l}}}\right), \qquad (13)$$

where m represents the gas mass produced by evaporation of liquid on the interface of unit area in unit time, which can be calculated by the equation at the right end of the equal sign of the following formula. Meanwhile, in order to facilitate the treatment in the simulation process, the temperature of the gas–liquid interface is approximately treated, and the interface temperature is set as the saturation temperature T_{s} of the liquid. Moreover, the phenomenon of liquid evaporation occurs when the liquid temperature at the interface is higher than the saturation temperature of the liquid. After approximate processing, it can be described by the following formula:

$$m=-\left(\frac{M_{\mathrm{w}}}{\Delta H_{\mathrm{gl}}}\right)\boldsymbol{n}\cdot k\nabla T\approx C\rho_{\mathrm{l}}\frac{(T-T_{\mathrm{s}})}{T_{\mathrm{s}}}, \qquad (14)$$

where the constant term C takes the value of 0.03.

In the simulation, the heat transfer control equation of gas–liquid two-phase can be described by the following formula:

$$\rho C_{\mathrm{p}}\left[\frac{\partial T}{\partial t}+\left(\boldsymbol{v}\cdot\nabla\right)T\right]=-\nabla\cdot k\nabla T, \qquad (15)$$

where C_{p} represents specific heat capacity, k represents thermal conductivity.

In order to ensure the accuracy of the model, the phase change latent heat term is added to the convection conduction equation to obtain

$$\rho C_{\mathrm{p}}\left[\frac{\partial T}{\partial t}+(\boldsymbol{v}\cdot\nabla)T\right]=-\nabla\cdot k\nabla T-\frac{m\delta\Delta H_{\mathrm{gl}}}{M_{\mathrm{w}}},\tag{16}$$

where ΔH_{gl} represents the enthalpy of vaporization, $M_{\mathrm{w}}=0.018$ kg/mol represents the molar mass of gas molecules.

In addition, the shear stress on the gas–liquid interface caused by Marangoni convection due to the difference of temperature distribution in the boiling process can be expressed as

$$\boldsymbol{F}=\left\{\begin{array}{l}\dfrac{\mathrm{d}\vartheta}{\mathrm{d}T}\cdot\Delta T_x\cdot\delta\\[2ex]\dfrac{\mathrm{d}\vartheta}{\mathrm{d}T}\cdot\Delta T_y\cdot\delta\end{array}\right\},\tag{17}$$

where the temperature gradient of surface tension $\mathrm{d}\vartheta/\mathrm{d}T=-1.8\times10^{-4}$ N/(m·K), ΔT_x represents the temperature difference along the x-axis direction and ΔT_y represents the temperature difference along the y-axis direction.

The phase field function ϕ is introduced to track the gas–liquid interface. The phase field function is solved by the phase field equation and the obtained velocity and pressure field distribution

$$\frac{\partial\phi}{\partial t}=\frac{\nabla}{\rho}\cdot\left\{\xi\left[\nabla v+(\nabla\boldsymbol{v})^{\mathrm{T}}\right]-P\boldsymbol{I}\right\}-(\boldsymbol{v}\cdot\nabla)\boldsymbol{v}+\frac{1}{\rho}\boldsymbol{F}.\tag{18}$$

For the gas–liquid phase transition in the boiling process, the continuity equation with phase transition is introduced by the phase field method in this study

$$\frac{\partial\phi}{\partial t}+\boldsymbol{v}\cdot\nabla\phi-m\delta\left(\frac{V_{\mathrm{f,g}}}{\rho_{\mathrm{g}}}+\frac{V_{\mathrm{f,l}}}{\rho_{\mathrm{l}}}\right)=\nabla\cdot\frac{M\lambda}{h^2}\nabla\varphi,\tag{19}$$

where M represents the phase field mobility, h represents the thickness of the two-phase transition region, $V_{\mathrm{f,g}}$ and $V_{\mathrm{f,l}}$ represent the volume ratio of gas phase and liquid phase, respectively. φ represents the relevant variable of solving the phase field, which can be obtained by the following formula:

$$\varphi=\phi\left(\phi^2-1\right)-\nabla\cdot h^2\nabla\phi,\tag{20}$$

and in the model, the temperature of the heating surface is uniform and constant, and the contact angle between the gas–liquid interface and the heating surface is a fixed value, which is not changed by the movement of the three-phase contact line.

2.2. Initial condition setting

This study simulates the nucleation and growth process of bubble during boiling heat transfer. In order to explore the influence of different parameters on bubble growth and evolution, we use the two-dimensional axisymmetric calculation region shown in Fig. 1 for simulation. Calculation area is $x\times y=6$ cm $\times$ 12 cm rectangle, when $t=0$, we set a quarter round steam chamber with radius $r=0.1$ cm at $x=0$, $y=0$. In the simulation, the initial simulation conditions set the latent heat of evaporation to $(4200/M_{\mathrm{w}})$ J/mol and the saturation temperature $T_{\mathrm{s}}=373.15$ K.

As shown in Fig. 1, we set the left axis of the rectangular calculation area to always be axisymmetric boundary, the remaining three axes of the rectangular calculation area are set as the following boundary conditions in the process of gas–liquid two-phase flow and convection conduction, respectively. (i) In the process of gas–liquid two-phase flow, this paper sets the upper axis of the calculation area as the outlet boundary without viscous stress, the right axis as the ideal non slip boundary, that is, $\boldsymbol{v}=0$, and the lower axis as the wetting boundary. At the initial time t_0, we set the simulation conditions as $\boldsymbol{v}(t_0)=0$, $P(t_0)=0$. (ii) In the process of convection conduction, both the upper axis and the right axis are set as thermal insulation boundaries, and the lower axis is set as the third type of heat transfer boundary conditions. The orange boundary in Fig. 1 represents the solid–liquid interface in the simulation process, and the green boundary represents the gas–liquid interface, the included angle from the gas–liquid interface to the solid–liquid interface is the contact angle of the heating surface θ.

In the simulation, we focus on the base diameter and bubble height during the growth of the steam chamber as shown in the figure. The physical parameters used in the simulation are shown in Table 1.

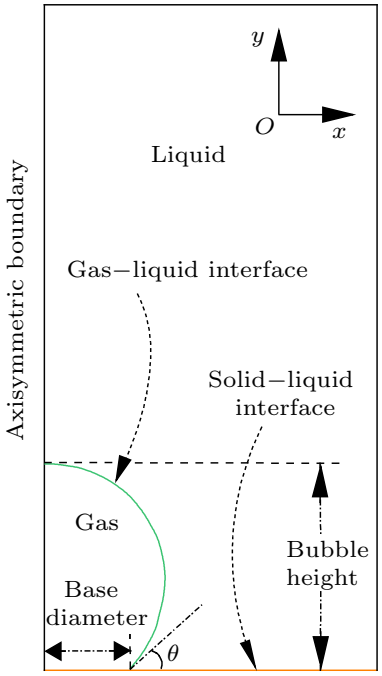


Fig. 1. Schematic diagram of simulation area.

Table 1. Material physical parameters.

Property	Symbol	Gas	Liquid
Specific heat	C_p (J/(kg·K))	1840	4200
Thermal conductivity	k (W/(m·K))	$8.3154\times10^{-5}\cdot T-7.4556\times10^{-3}$	0.63
Kinetic viscosity	μ (Pa·s)	4.0×10^{-5}	1.0×10^{-3}
Density	ρ (kg/m^3)	$(p+p_0)\cdot M_w/8.314/T$	1.0×10^3

3. Results and discussion

In this paper, we establish a bubble growth model under microgravity, and in this model, we use the dimensionless form in the solution process. This study simulates the nucleation, growth, deformation and detachment process of a single bubble under different gravity conditions, undercooling conditions and contact angles, and explores the evolution law under different conditions. In this work, T_w represents wall superheat, θ represents the contact angle, g_z represents the gravity level, T_{sub} represents liquid supercooling.

3.1. Morphological evolution of a single bubble in microgravity

Figure 2 shows the evolution of a single bubble when $T_{sub}=0$ K, $T_w=5.5$ K, $g_z/g=0.04$, $\theta=50°$, the red area in the figure indicates the growth of bubbles, and the blue area is the liquid phase area. Figure 2(a) shows the growth morphology of the bubble at the time of 0.01 s. In this stage, the bubbles grow rapidly on the heating surface, the red area gradually expands, and both the bubble height and base diameter are in the expansion stage. When the bubble grows to 0.25 s, the height of the bubble is still growing, but the bottom of the bubble begins to shrink, as shown in Fig. 2(b), and at this time, the bubble height is 1.38 cm, the base diameter reaches the maximum value of 0.57 cm during the growth process. From 0.25 s to 0.49 s, the bubble height still increases, but unlike the previous stage, the base diameter gradually decreases until the bubble left the heating interface. Figure 2(c) is the last time when the bubbles leave, and the bubble height is 2.34 cm at this time. Figure 2(d) shows the shape of the bubbles at 0.40 s, when the bubbles are completely separated from the heating interface. During the whole growth process, the bubble height keeps increasing, while the base diameter shows a trend of first increasing and then decreasing. The gas–liquid interface gradually extends to the liquid phase, and the bubble shape gradually becomes an elliptical shape, and finally the bubble separates from the heating interface.

In order to explore the change law of bubble shape during bubble growth under low microgravity conditions, we further carry out quantitative research, as shown in Fig. 3, the function of bubble height and base diameter with time, where the orange curve represents the base diameter. At $t=0.25$ s, the bottom diameter of the bubble reaches the maximum value, that is, the base diameter of the bubble first increases and then decreases. Specifically, the size of the base diameter of the bubble expands slowly on the heating surface within 0 s–0.25 s, the bottom diameter increases from the initial 0.10 cm to 0.57 cm, and then begins to reduce the bottom diameter within 0.25 s–0.49 s, from 0.57 cm to 0 cm. Finally, the bubble separates from the heating surface, and the bottom diameter of the bubbles is 0 cm. The bubble height increases from bubble nucleation to final separation, as shown by the green curve in Fig. 3. This result is generally consistent with the results of Dhir *et al.*[9] in NASA microgravity physics laboratory. In order to facilitate simulation and quantitative research, the model in this paper does not consider the dynamic contact angle between the bubble and the heating surface, but adopts a static contact angle of 50°. On the whole, this simulation can completely reproduce the evolution law of bubbles from initial nucleation to final separation from the heated surface. And the model has good consistency and accuracy compared with classical experiments.

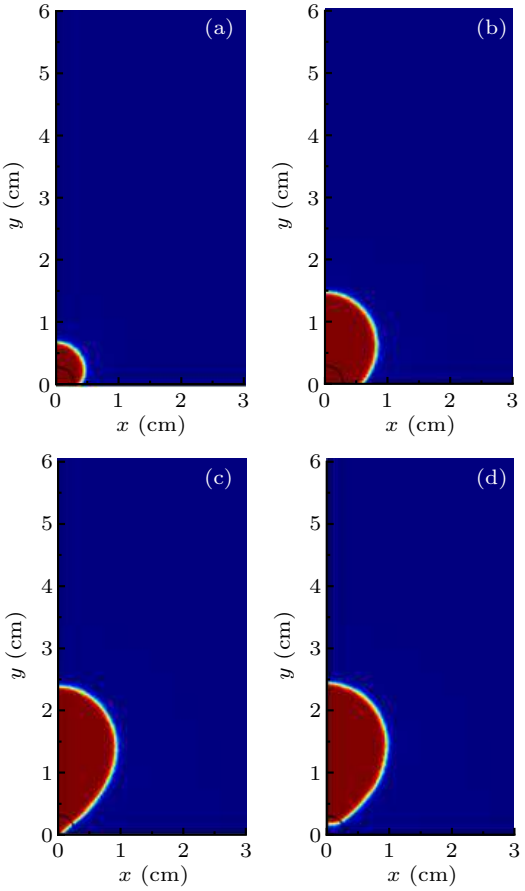


Fig. 2. Bubble shape at time (a) $t=0.01$ s, (b) $t=0.25$ s, (c) $t=0.39$ s, (d) $t=0.40$ s.

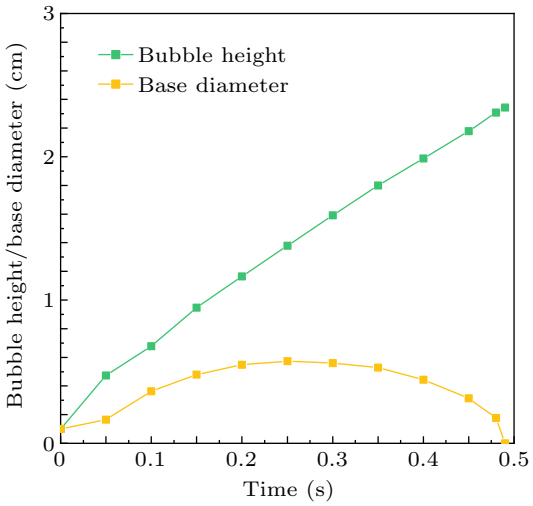


Fig. 3. Bubble height and base diameter as a function of time.

3.2. Effect of liquid subcooling on bubble growth

Figure 4 shows the change process of bubble height and bubble base diameter with time when other conditions are the same, while the liquid undercooling is different. Lines of the same color in the Fig. 4 represent bubble height and base diameter under the same simulation conditions. It can be seen from the figure that with the increase of liquid undercooling, the bubble growth rate decreases and the bubble growth cycle increases. When the liquid undercooling is 1 K, the time for bubble to finally leave the heating interface is 3.31 s, while when the liquid undercooling increases to 9 K, the departure time for bubble becomes 4.23 s. At the same time, the maximum value of bubble base diameter also changes under different liquid subcooling degrees. It is obvious from the curve showing bubble base diameter in the figure that with the increase of undercooling, the base diameter gradually decreases. When the liquid undercooling is 1 K, the base diameter begins to shrink gradually when it reaches 3.69 cm, while when the liquid undercooling is 9 K, the maximum value that the bubble base diameter can reach is 3.36 cm. The value of bubble height always shows an increasing trend in the whole growth process, and it can be seen from the figure that the smaller the liquid undercooling, the smaller the value of bubble height. At the time of $t = 3$ s, the value of bubble height is 9.87 cm, 9.56 cm, and 9.41 cm when the liquid undercooling is 1 K, 2 K, and 3 K, respectively. Generally speaking, we can conclude that under microgravity conditions, with the increase of liquid undercooling, the bubble growth cycle time increases, while the maximum value of base diameter will decrease with the increase of liquid undercooling. Furthermore, Table 2 compares the maximum base diameter of bubble before gradually shrinking and the maximum height before bubble lift off under the same other conditions and different degrees of undercooling, we find that under low microgravity, the base diameter of bubbles shows a dynamic change of expansion and contraction, and generally, when the base diameter of bubbles expands until it reaches 30%–40% of the maximum bubble height, the base diameter will shrink, and finally the bubbles will lift off.

Figure 5 describes the change of bubble departure time and bubble height at liftoff with liquid undercooling. The pink curve in Fig. 5 represents the time when the bubble finally leaves the heating surface after boiling, and the green curve represents the bubble height corresponding to the departure time. It is obvious that the pink curve shows a very clear upward trend. When the liquid undercooling is 4 K and 8 K, the corresponding bubble department time is 3.8 s and 4.08 s respectively, which means that under the same gravity level and system pressure, with the increase of liquid undercooling, the departure time of bubbles gradually increases, and we can find from the figure that the greater the undercooling, the more obvious this phenomenon is. The green curve is always at a relatively stable level, and with the increase of liquid undercooling, its value is always about 9.5 cm. The green curve has little fluctuation, and the value is generally stable, which means that the change of bubble height with undercooling is not very obvious, and the size of liquid undercooling has no significant effect on bubble height at the time of liftoff.

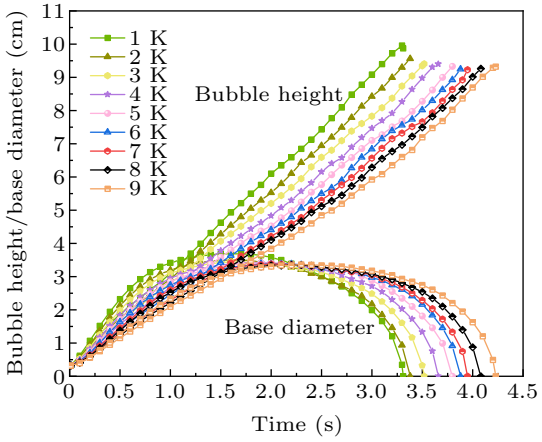


Fig. 4. Bubble height and base diameter with time at different liquid subcooling degrees.

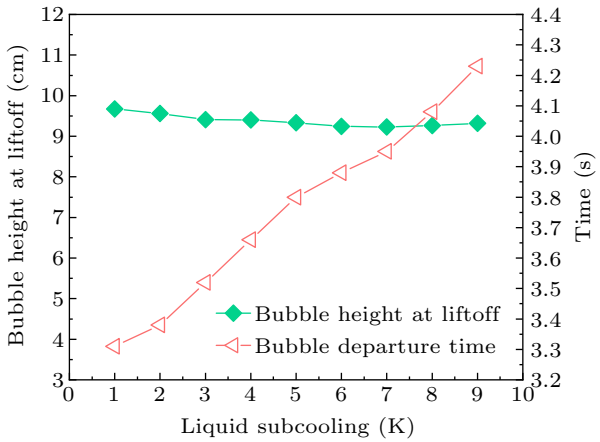


Fig. 5. Variation of bubble departure time and bubble height at liftoff with undercooling.

Table 2. Maximum base diameter and bubble height under different undercooling.

Undercooling	1 K	2 K	3 K	4 K	5 K	6 K	7 K	8 K	9 K
Bubble height (cm)	9.87	9.56	9.41	9.40	9.33	9.24	9.23	9.26	9.32
Base diameter (cm)	3.69	3.50	3.45	3.42	3.41	3.38	3.38	3.35	3.36
Base diameter/bubble height (%)	37.39	36.61	36.63	36.38	36.55	36.58	36.62	36.18	36.05

3.3. Effect of contact angle on bubble growth

Figure 6 shows the changes of bubble height and bubble base diameter with time under different contact angles, in which the green curve, blue curve and orange curve represent bubble height and base diameter at $\theta = 80°$, respectively. We can find that at the initial stage of bubble growth, the bubble height and base diameter at different contact angles are not much different. With the passage of time, the bubble height at different contact angles is relatively close, but the base diameter difference is very obvious. When the contact angle is 80°, it can be seen from the green curve in Fig. 6 that the base diameter of the bubble is 0 cm at $t = 2.63$ s, which means that the bubble leaves the heating surface, and at this time, the bubble height is 8.32 cm. When the contact angle is 90°, it can be seen from the blue curve that within 0 s–1.52 s, the base diameter gradually increases with time, and after $t = 1.52$ s, the value of base diameter gradually decreases and the bubble shrinks. When $t = 3.14$ s, the bubble leaves the heating surface, and the bubble height at this time is 9.68 cm. When the contact angle is 95°, the changes of bubble height and base diameter with time are shown in the orange curve, at $t = 1.3$ s, the curve of bubble height intersects with the curve of base diameter. Before this intersection, the value of base diameter is greater than that of bubble height, and then the value of bubble height is significantly greater than that of base diameter, which is similar to the others two curves.

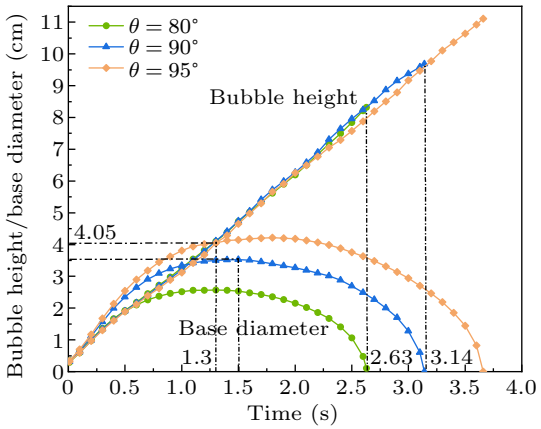


Fig. 6. Bubble height and base diameter as a function of the contact angle.

In order to get a clearer relationship between contact angle and bubble shape, we simulate the bubbles under different contact angles, the results are shown in Fig. 7. We can find that the bubble morphology at the same time with contact angles of 80°, 90°, and 95° respectively. It can be seen from the figure that when the contact angle is 95°, the base diameter of the bubble is significantly larger than that when the contact angle is 90° or 80°, but the bubble height values of the three are not different. Through the above analysis, we can conclude that with the increase of contact angle, the bubble growth cycle gradually becomes larger, meanwhile the larger the contact angle is, the larger the base diameter on the heating surface is.

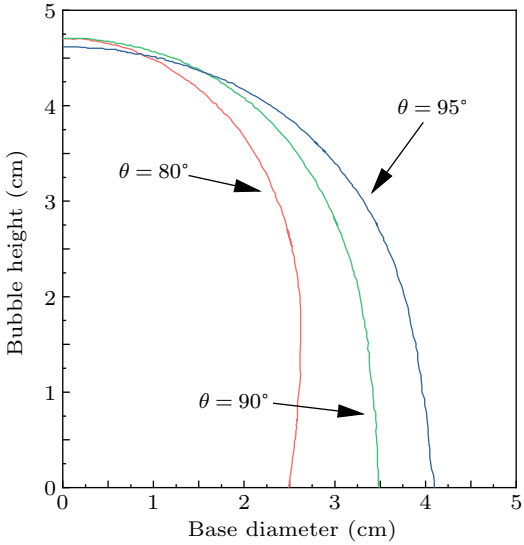


Fig. 7. Bubble morphology with different contact angles at the same time.

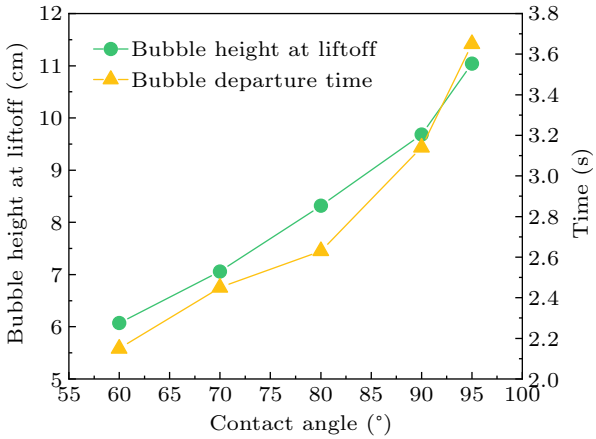


Fig. 8. Bubble height at liftoff and departure time as a function of the contact angle.

Figure 8 shows the changes of bubble height and departure time at the contact angle of 60°, 70°, 80°, 90°, and 95° at the gravity level of $0.007\boldsymbol{g}$, respectively. The yellow curve represents bubble department time, and the green curve represents bubble height at liftoff. It can be seen from the figure that both the yellow curve and the green curve show an upward trend with the increase of time, and the rising range is basically

similar, which indicates that the bubble height and departure time increase with the increase of contact angle. The increase of bubble departure time may be due to the increase of surface tension to maintain the stable shape of bubbles when the angle of contact angle increases, which will make it more difficult for bubbles to separate, resulting in longer bubble separation time.

3.4. Effect of gravity level on bubble growth

Figures 9(a) and 9(b) show the shape of the bubbles leaving the heating front and the bubble height throughout the growth process at different gravity levels, respectively. The dotted lines with different colors in Fig. 9(a) are the same for other simulation conditions, but the bubbles leave the heating surface under different gravity level conditions. According to the research of Zhao and Du *et al.*[27,28] and their qualitative comparison with the RKM model, we choose the gravity levels as $0.08\boldsymbol{g}$, $0.06\boldsymbol{g}$, $0.04\boldsymbol{g}$, $0.02\boldsymbol{g}$, $0.01\boldsymbol{g}$, $0.008\boldsymbol{g}$, $0.006\boldsymbol{g}$, and $0.004\boldsymbol{g}$, respectively. It can be clearly seen from the shape of the bubble in the Fig. 9(a) that the shape of the bubble under the condition of $0.08\boldsymbol{g}$ is the smallest, and the shape of the bubble under the condition of $0.004\boldsymbol{g}$ is the largest, and the shape and size of the bubble before take-off is inversely proportional to the level of gravity, that is the higher the gravity level, the smaller the shape of the bubble. Figure 9(b) is the change curve of bubble height with time under the gravity condition corresponding to Fig. 9(a). We can see from the Fig. 9(b) that in the early stage of bubble growth, the bubble height under different gravity conditions is not very different, and the curves in the figure almost overlap. During the later stages of bubble growth, the distance between the curves gradually widens, especially before the bubble lifts off. In addition, we take the radius of a circle as the bubble departure radius R, and the area of this circle is equal to the bubble area at the time of departure, then we study the relationship between the bubble departure radius and different gravity levels. The simulation results are shown in Fig. 10(a). It can be clearly seen from Fig. 10(a) that with the increase of gravity level, the bubble departure radius gradually decrease. We can obtain the curve shown in Fig. 10(b) by further analyzing of this law, that is, the bubble departure radius R is proportional to $\boldsymbol{g}^{-1/2}$.

Figure 11 shows a single bubble morphological evolution under the condition of $\theta = 50°$, $T_{\rm w} = 10$ K, $T_{\rm sub} = 0$, $\boldsymbol{g}_z/\boldsymbol{g} = 0.006$. Because the growth cycles of bubbles under different gravity levels are similar, and at the same time, in order to express the research law more clearly, we use the growth process of a single bubble at a gravity level of $0.006\boldsymbol{g}$ to study. The bubble shape in Fig. 11 is the shape of the bubble every 0.5 s after the start of the simulation and the shape of the bubble when it finally leaves the heating surface, and its bubble height corresponds to the blue line in Fig. 9(b). In the initial

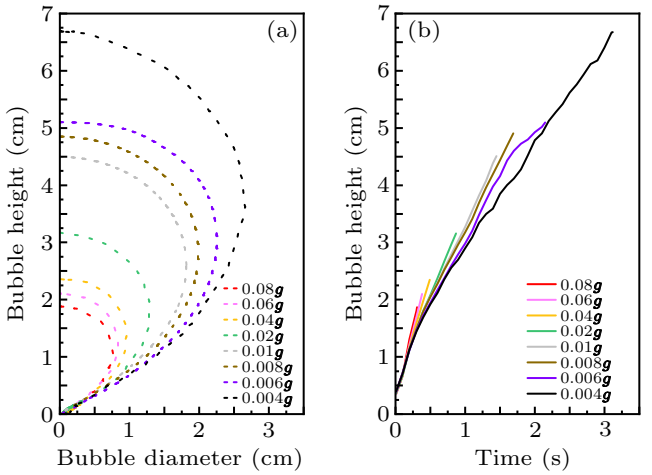


Fig. 9. (a) Bubble shapes at liftoff under different gravity levels. (b) Bubble equivalent diameter as a function of the growth time.

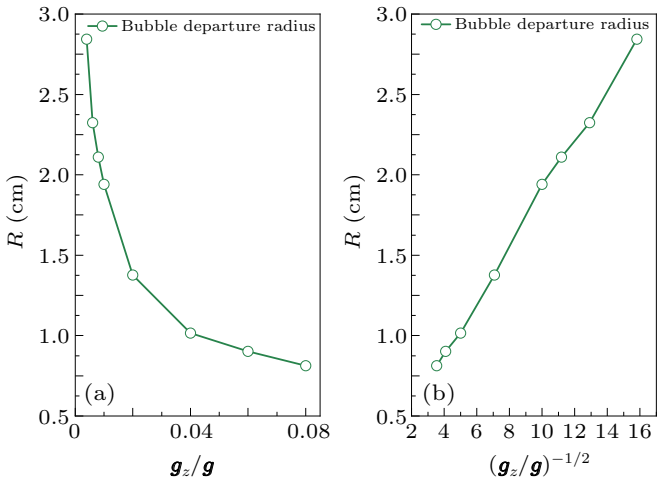


Fig. 10. (a) The variations of bubble departure radius with gravity level. (b) The variations of bubble departure radius with $\boldsymbol{g}^{-1/2}$.

stage of bubble growth, bubbles grow rapidly on the heated surface. As the height of the bubble increases, the base diameter of the bubble also increases. But the base diameter of the bubble begins to shrink after reaching the maximum size until it leaves the heating surface, but the height of the bubble continues to rise. When the base diameter of the bubble reaches the maximum size, the shape of the bubble is shown by the red dotted line in Fig. 11, and its radius value is 1.53 cm. Then, the bottom of the bubble begins to shrink, and the height of the bubble increases as the bottom shrinks. Finally, the bubble leaves the heating surface in the shape shown by the black dotted line in Fig. 11. In Fig. 9(b), the corresponding bubble height is 5.08 cm, and the diameter of the bottom of the bubble is 30.12% of the height of the bubble. Under the action of surface tension, bubbles separate from the heated surface and produce new nucleation points. And the cycle behavior of bubble nucleation, growth, deformation and detachment will be repeated. Combined with Figs. 9 and 11, we can conclude that in the early stage of bubble growth, the influence of gravity level on bubble shape is not obvious. From the perspective

of bubble growth morphology, the bubble growth law under different gravity levels is similar as a whole, but the bubble diameter and growth time will increase with the decrease of gravity level.

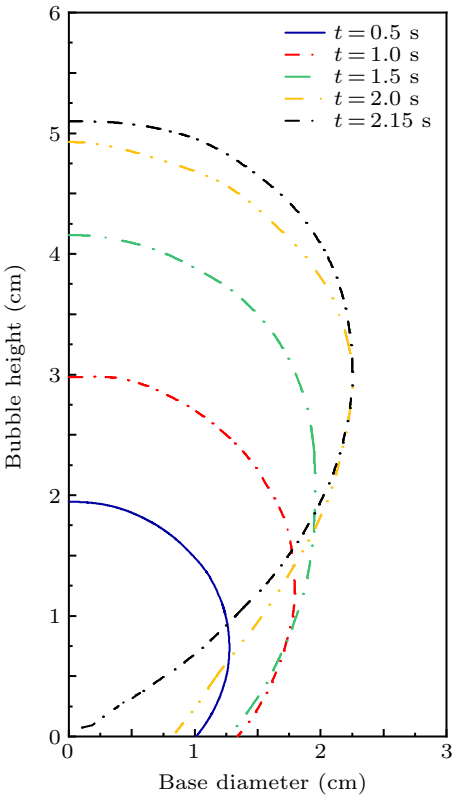


Fig. 11. Dynamic evolution of single bubble at 0.006$\boldsymbol{g}$ gravity.

4. Conclusion

In this study, we take single bubble pool boiling as the model system of nucleate boiling phenomenon, numerically study the nucleation, growth, deformation and abscission process of single bubble by using phase field method. Based on the model, we analyze the effects of liquid undercooling, contact angle and gravity level on bubble growth process and desorption characteristics. Through the study of the established model, we draw the following conclusions.

(i) In the low microgravity condition, the bubble growth process is accompanied by the dynamic changes of the expansion and contraction of the bubble base, which shows that the bubble base expands to 30%–40% of the maximum height of the top of the bubble and begins to shrink until it detaches, which is consistent with the experimental results.

(ii) And the simulation results show that the liquid subcooling degree has no significant effect on the bubble height, but with the increase of the subcooling degree, the bubble growth time will increase significantly. At the same time, the bubble height and departure time are also affected by the contact angle between the solid–liquid–gas three phases. With the increase of the solid–liquid–gas contact angle, the bubble height and departure time both increase.

(iii) In addition, we find that the bubble departure radius R is proportional to $g^{-1/2}$, and the bubble height and growth time decrease with the increase of gravity. At different low microgravity levels, the bubble height and growth time show similar laws with the change of gravity level.

Acknowledgments

Project supported by the National Natural Science Foundation of China (Grant Nos. 52161002, 51661020, and 11364024), the Postdoctoral Science Foundation of China (Grant No. 2014M560371), and the Funds for Distinguished Young Scientists of Lanzhou University of Technology of China (Grant No. J201304).

References

[1] Son G, Dhir V and Ramanujapu N 1999 *J. Heat Transf. Trans. ASME* **121** 623
[2] Lee R and Nydahl J 1989 *J. Heat Transf. Trans. ASME* **111** 474
[3] Nam Y, Wu J, Warrier G and Ju Y S 2009 *J. Heat Transf. Trans. ASME* **131** 121004
[4] Qiu D M, Dhir V K, Hasan M M, Chao D F, Neumann E, Yee G and Birchenough A 2000 *Microgravity Fluid Physics & Heat Transfer*
[5] Straub J 2001 *Adv. Heat Transf.* **35** 57
[6] Lee H C, Do Oh B, Bae S W and Kim M H 2003 *Int. J. Multiph. Flow* **29** 1857
[7] Henry C D, Kim J, Chamberlain B and Hartman T G 2005 *Exp. Therm. Fluid Sci.* **29** 773
[8] Zhao J F, Li J, Yan N and Wang S F 2010 *Chin. Phys. Lett.* **27** 076401
[9] Dhir V K, Warrier G R, Aktinol E, Chao D, Eggers J, Sheredy W and Booth W 2012 *Microgravity Sci. Technol.* **24** 307
[10] Nejati I, Sielaff A, Franz B, Zimmermann M, Hänichen P, Schweikert K, Krempel J, Stephan P, Martin A, Scheerer H, Engler T and Oechsner M 2020 *Microgravity Sci. Technol.* **32** 597
[11] Li D and Dhir V K 2007 *J. Heat Transf. Trans. ASME* **129** 864
[12] Pu L, Li H, Lv X, Zhao J, Chen T and Zhu Y 2008 *Microgravity Sci. Technol.* **20** 247
[13] Shu S and Yang N 2013 *Ind. Eng. Chem. Res.* **52** 11391
[14] Urbano A, Tanguy S, Huber G and Colin C 2018 *Int. J. Heat Mass Transf.* **123** 1128
[15] Li Z D, Zhang L, Zhao J F, Li H X, Li K and Wu K 2015 *Int. J. Heat Mass Transf.* **84** 409
[16] Zhang L, Li Z D, Li K, Li H X and Zhao J F 2015 *Appl. Therm. Eng.* **88** 118
[17] Murallidharan J, Giustini G, Sato Y, Ničeno B, Badalassi V and Walker S P 2016 *Nucl. Eng. Technol.* **48** 859
[18] Liu J, Wang G, Zhang L, Shi Y, Zhang H and Yao S C 2017 *Propuls. Power Res.* **6** 117
[19] Cheng N, Guo Y and Peng C 2019 *Ann. Nucl. Energy* **124** 179
[20] Voglar J 2022 *Fluids* **7** 90
[21] Takada N, Misawa M and Tomiyama A 2005 *Fluids Engineering Division Summer Meeting*, June 19–23, 2005, Houston, USA, pp. 259–264
[22] Zhu C S, Han D and Xu S 2018 *Chin. Phys. B* **27** 094704
[23] Wang Z, Zheng X and Karniadakis G 2020 *Fluids Engineering Division Summer Meeting*, July 13–15, 2020, p. FEDSM2020-20176
[24] Yi T H, Lei Z S and Zhao J F 2019 *Int. J. Heat Mass Transf.* **132** 1176
[25] Mianmahale M A, Mehrabani-Zeinabad A, Zare M H and Ghadiri M 2021 *NPJ Microgravity* **7** 1
[26] Rivera-Salinas J E, Gutiérrez-Pérez V H, Vargas-Ramírez M, Gregorio-Jáuregui K M, Cruz-Ramírez A, Avalos-Belmontes F, Ortíz-Cisneros J C and Escobedo-Bocardo J C 2014 *Mater. Res.* **17** 1550
[27] Zhao J F, Zhang L, Du W F and Li H X 2021 *Acta Aerodyn. Sin.* **39** 121
[28] Du W F and Zhao J F 2019 *Chin. Sci. Bull.* **65** 1629